Solution of Reduced Resistive Magnetohydrodynamics using Implicit Adaptive Mesh Refinement

B. Philip[1], M. Pernice[1], and L. Chacón[2]

[1] Computer and Computational Sciences Division, Los Alamos National Laboratory, Los Alamos, NM 87545 {bphilip,pernice}@lanl.gov
[2] Theoretical Division, Los Alamos National Laboratory, Los Alamos, NM 87545 chacon@lanl.gov

Summary. Computational study of the macroscopic stability of plasmas is a challenging multi-scale problem. Implicit time integration can be used to relieve stability constraints due to fast Alfvén waves, and adaptive mesh refinement (AMR) can be used to resolve highly localized solution features. The strong nonlinearities and numerical stiffness of magnetohydrodynamics (MHD) models present further challenges that must be solved to make implicit AMR practical. We present initial results on the application of implicit AMR to a reduced resistive MHD model.

1 Introduction

Magnetohydrodynamics (MHD) models are useful for studying the macroscopic behavior of plasmas. Plasmas exhibit a wide range of complex behavior, including magnetic reconnection, where the magnetic field undergoes a rapid reconfiguration accompanied by conversion of energy stored in the magnetic field to kinetic energy. Reconnection is associated with the formation of thin, localized current sheets, which nevertheless profoundly influence macroscopic behavior. Thus, it is natural to consider adaptive mesh refinement (AMR) to locally resolve these features.

MHD models also display behaviors that occur over a wide range of time scales, many of which are much faster than the time scale over which reconnection occurs. Time integration methods that are subject to stability constraints that arise from the fastest time scales are inappropriate for simulation-based study of reconnection phenomena. We therefore employ implicit time integration methods where time steps are constrained only by accuracy, not stability.

Implicit time integration requires the solution of large-scale systems of nonlinear equations at each time step, and fast, robust solution methods are necessary for implicit methods to be practical. Fortunately, Newton-Krylov methods [2] have met this requirement in a variety of contexts [6], provided

effective preconditioning is used. In particular, we have demonstrated excellent preconditioner performance for reduced MHD models [4, 3]. The key to this success is the design of physics-based preconditioners that preserve important couplings between variables and allow the effective use of multigrid methods. On AMR grids, fast multilevel methods that exploit the structure of the mesh are needed.

2 Adaptive Mesh Refinement

We use *structured* AMR (SAMR), in which the grid is organized as a collection of refinement levels. Each refinement level is the union of rectangular patches having fixed resolution, and is fully nested in the next coarser level (except at physical boundaries); see Figure 2 for some examples. This hierarchical structure naturally lends itself to domain decomposition, by treating each refinement level as a separate subdomain and exploiting the natural partition of each level by its patches. The fully overlapping nature of the domains enables use of coarse grid points that are covered by a finer level to accelerate the solution process. In particular, we use the Fast Adpative Composite grid (FAC) method [7], which is a multiplicative approach that treats levels sequentially, analogous to a multigrid V-cycle. FAC can employ simple smoothing on refinement levels, and an approximate solve on the coarsest, global level.

SAMR requires special discretization procedures to enforce smoothness of the solution at the interfaces between coarse and fine regions. Continuity of the solution at coarse/fine interfaces is ensured by providing each level with Dirichlet boundary conditions that are determined from piecewise quadratic interpolation of data from the next coarser level. Flux continuity at coarse/fine interfaces is enforced by using this Dirichlet data to compute $\mathcal{O}(h^3)$-accurate gradients normal to the level boundary. Nevertheless, careful selection of the MHD model is required to successfully use SAMR in this context.

3 Current-Vorticity Formulation of Reduced MHD

The two-dimensional reduced MHD formalism assumes that the plasma is strongly magnetized by a large magnetic field in the (ignorable) z-direction [5]. It follows that the dynamics is restricted to the $x-y$ plane, where the plasma is incompressible. This allows descriptions of the plasma velocity $\mathbf{v} = (u, v)^\mathsf{T}$ in terms of a streamfunction Φ (with $u = -\Phi_y$ and $v = \Phi_x$) and the magnetic field $\mathbf{B} = (B_1, B_2)^\mathsf{T}$ in terms of a poloidal flux function Ψ (with $B_1 = -\Psi_y$ and $B_2 = \Psi_x$). This leads to the streamfunction-vorticity formulation

$$\begin{aligned} \partial_t \omega + \mathbf{v} \cdot \nabla \omega - \nu \nabla^2 \omega &= \mathbf{B} \cdot \nabla J \\ \partial_t \Psi + \mathbf{v} \cdot \nabla \Psi - \eta \nabla^2 \Psi &= 0 \\ \nabla^2 \Phi &= \omega \end{aligned} \tag{1}$$

where ω is the vorticity, $J = \nabla^2\Psi$ is the electric current, ν is the viscosity, and η is the resistivity. While this formulation was successfully treated in [4], it is not well-suited to SAMR, because of the need to compute $J = \nabla^2\Psi$ at coarse/fine interfaces, even if much higher-order interpolation is used. The fact that J is determined by differentiation leads to small instabilities along the coarse/fine interface that grow as the simulation proceeds. Similar difficulties were reported in [9] for ideal MHD on unstructured grids. Instead, and following [9], we use a current-vorticity formulation

$$\begin{aligned} \partial_t J + \mathbf{v}\cdot\nabla J - \eta\nabla^2 J - \mathbf{B}\cdot\nabla\omega &= \{\Phi,\Psi\} \\ \partial_t \omega + \mathbf{v}\cdot\nabla\omega - \nu\nabla^2\omega - \mathbf{B}\cdot\nabla J &= 0 \\ \omega - \nabla^2\Phi &= 0 \\ J - \nabla^2\Psi &= 0 \end{aligned} \tag{2}$$

where $\{\Phi,\Psi\} = 2[\Phi_{xy}(\Psi_{xx}-\Psi_{yy}) - \Psi_{xy}(\Phi_{xx}-\Phi_{yy})]$.

Our main task here is to extend the physics-based preconditioner developed in [4] to handle (2). For the sake of brevity, we assume the reader is familiar with the derivation in [4], and do not repeat it here. Discretizing (2) in time with a theta difference scheme yields

$$\begin{aligned} (J^{n+1}-J^n)/\Delta t + [\mathbf{v}\cdot\nabla J]^{n+\theta} - \eta\nabla^2 J^{n+\theta} - [\mathbf{B}\cdot\nabla\omega]^{n+\theta} &= \{\Phi,\Psi\}^{n+\theta} \\ (\omega^{n+1}-\omega^n)/\Delta t + [\mathbf{v}\cdot\nabla\omega]^{n+\theta} - \nu\nabla^2\omega^{n+\theta} - [\mathbf{B}\cdot\nabla J]^{n+\theta} &= 0 \\ \omega^{n+\theta} - \nabla^2\Phi^{n+\theta} &= 0 \\ J^{n+\theta} - \nabla^2\Psi^{n+\theta} &= 0 \end{aligned} \tag{3}$$

where $n+\theta$-level quantities are calculated as $\xi^{n+\theta} = (1-\theta)\xi^n + \theta\xi^{n+1}$. Backward Euler time discretization is obtained by $\theta = 1$ and Crank-Nicolson time discretization corresponds to $\theta = 1/2$. We represent (3) generically by $\mathbf{G}(\mathbf{x}^{n+1}) = 0$ and compute the time-advanced solution with a Jacobian-free Newton-Krylov (JFNK) method.

Each iteration of JFNK requires solution of the linearized system

$$\mathcal{L}_\eta\delta J + \theta(\delta\mathbf{v}\cdot\nabla J_0 - \mathbf{B_0}\cdot\nabla\delta\omega - \delta\mathbf{B}\cdot\nabla\omega_0 - \{\delta\Phi,\Psi_0\} - \{\Phi_0,\delta\Psi\}) = -G_J \tag{4}$$

$$\mathcal{L}_\nu\delta\omega + \theta(\delta\mathbf{v}\cdot\nabla\omega_0 - \mathbf{B_0}\cdot\nabla\delta J - \delta\mathbf{B}\cdot\nabla J_0) = -G_\omega \tag{5}$$

$$\delta J - \nabla^2\delta\Psi = -G_\psi \tag{6}$$

$$\delta\omega - \nabla^2\delta\Phi = -G_\phi \tag{7}$$

where $\mathcal{L}_\alpha = \frac{1}{\Delta t} + \theta(\mathbf{v}_0\cdot\nabla - \alpha\nabla^2),\ \alpha = \eta,\nu$. Quantities with subscript 0 refer to solution quantities at the previous Newton iterate and $(G_J, G_\omega, G_\psi, G_\phi)^t$ refers to the nonlinear residual.

We extend the semi-implicit preconditioner for (1) to handle (2) by first substituting (6) and (7) in (4) and (5), respectively, and approximating as in [4], to obtain

$$\mathcal{P}\begin{pmatrix}\delta\Psi\\ \delta\Phi\end{pmatrix} \approx -\nabla^{-2}\left[\begin{pmatrix}G_J\\ G_\omega\end{pmatrix} - \mathcal{P}\begin{pmatrix}G_\Psi\\ G_\Phi\end{pmatrix}\right] \tag{8}$$

where

$$\mathcal{P} \equiv \begin{pmatrix} \mathcal{L}_\eta & -\theta \mathbf{B}_0 \cdot \nabla \\ -\theta \mathbf{B}_0 \cdot \nabla & \mathcal{L}_\nu \end{pmatrix}.$$

The system in (8) is only approximate, and is treated here as a predictor step for $\delta\Psi$ and $\delta\Phi$. Solution of (8) is done as described in [4], namely, by a few sweeps of the stationary method obtained by the splitting of $\mathcal{P}$ that is induced by separating $\mathcal{L}_\nu$ into its diagonal and off-diagonal parts, and forming the Schur complement of the split block matrix for inversion. After this, the system

$$\mathcal{P} \begin{pmatrix} \delta J \\ \delta\omega \end{pmatrix} = - \begin{pmatrix} G_J + \theta(\delta\mathbf{v} \cdot \nabla J_0 - \delta\mathbf{B} \cdot \nabla\omega_0 - \{\delta\Phi, \Psi_0\} - \{\Phi_0, \delta\Psi\}) \\ G_\omega + \theta(\delta\mathbf{v} \cdot \nabla\omega_0 - \delta\mathbf{B} \cdot \nabla J_0) \end{pmatrix} \quad (9)$$

is solved in the same manner for δJ and $\delta\omega$ using the predicted $\delta\Psi$ and $\delta\Phi$ in the right hand side.

4 Computational Results

We present initial results of applying implicit AMR to the classical tearing resistive instability problem described in [4]. The current-vorticity formulation (2) is used on the physical domain $\Omega = [0, 4] \times [0, 1]$, with periodic boundary conditions in x and homogeneous Dirichlet boundary conditions in y. Initial conditions are given by $\omega_0 = 0$ and a Harris current sheet $J_0 = \operatorname{sech}^2((y - 0.5)/\lambda)/\lambda$ with $\lambda = 0.2$. We use a fixed time step $\Delta t = 1$ and integrate to $t = 250$.

The software infrastructure described in [8] is used. In particular, we use the implementation of JFNK from PETSc's Scalable Nonlinear Equation Solver (SNES) package [1] with a constant forcing term, with both absolute and relative stopping tolerances of 10^{-4}. We developed implementations of FAC for solving the Poisson and convection-tensor diffusion sub-problems that are needed to implement the preconditioner [(8) and (9)].

Our criteria for dynamic mesh refinement are based on detecting solution features. Cells are selected for subdivision when $|J|$ exceeds 85% of its maximum value (following [9]) or when the curvature in ω exceeds 0.40. Regridding is done every fourth time step. These choices were determined experimentally to produce acceptable results. While a systematic study of the accuracy of the adaptive simulation is needed, Figure 1 shows good agreement of the growth of the magnetic perturbation calculated on different grid configurations with the same finest resolution. All these calculations predicted a growth rate of 0.046.

Figure 2 depicts evolution of the solution and grid for a 32×32 base grid with 3 refinement levels. Initially, refinement is concentrated in a strip surrounding $y = 0.5$ in order to resolve the current sheet. By $t = 120$ the magnetic island has opened up and the flow has organized itself into four

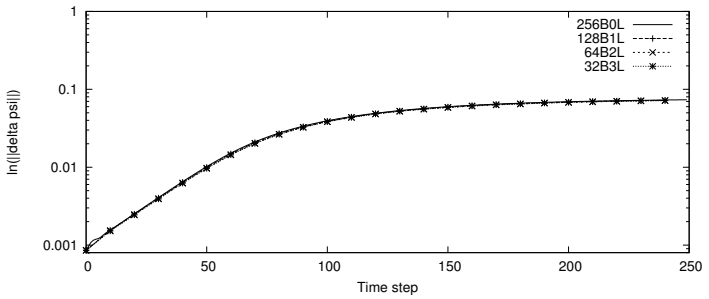

Fig. 1. Comparison of growth in $\delta\Psi$ for different grid configurations with the same finest resolution. The curves are labeled as "mBℓL", which indicates an $m \times m$ base grid and ℓ refinement levels.

distinct vortices of alternating sign. The mesh tracks the evolution of the solution, with refinement level 1 expanding to capture the magnetic island, de-refinement in the center of the island, and the remaining refinement levels focused on the vorticity. By $t = 200$, J has increased in the center of the magnetic island, and re-refinement has occurred to capture this behavior.

Finally, Table 1 shows the average number of nonlinear and linear iterations per time step as finer base grids and increasing numbers of refinement levels are used. The entries marked "–" are cases that were not run. The number of nonlinear iterations per time step is roughly constant for all cases. Reading horizontally, we note an increase in the number of linear iterations per time step as resolution is increased locally. This is consistent with the trend observed by reading vertically, where resolution is increased globally by using increasingly finer base grids. These trends are consistent with results found in [4], and are expected, because by increasing spatial resolution while running at a fixed time step, we are effectively running at larger multiples of the shear Alfvén wave explicit CFL limit. More importantly, reading diagonally (from lower left to upper right), we see that the number of linear iterations per time step is nearly constant for different grid configurations with a fixed finest resolution.

5 Conclusions

We have successfully demonstrated the use of implicit AMR for a reduced resistive model of MHD. The conventional streamfunction-vorticity formulation was found to be inappropriate for SAMR, but the current-vorticity formulation was shown to be amenable to this approach. Although a more formal accuracy study remains to be undertaken, we have demonstrated good agreement among predictions of the growth rate of the magnetic perturbation obtained from a variety of grid configurations having the finest resolution.

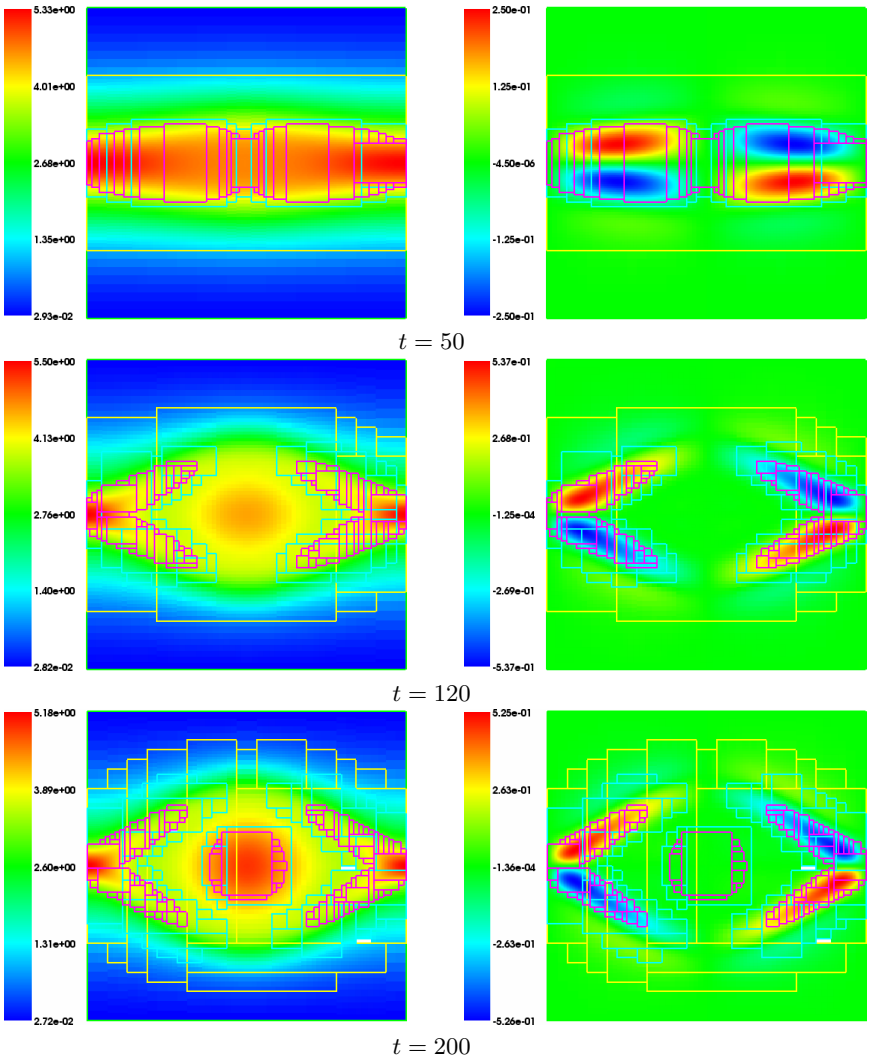

Fig. 2. Evolution of solution and grid over time . The y-axis is scaled by a factor of 4. The current J is on the left and the vorticity ω is on the right. The coarsest level is outlined in green; level 1: yellow; level 2: cyan; and level 3: magenta.

By using FAC to implement our physics-based preconditioner, we have shown that the number of linear iterations per time step at a given resolution is nearly constant, a property that is necessary for implicit AMR to achieve performance gains that are commensurate with the reduction in problem size made possible by local mesh refinement.

Table 1. Number of nonlinear iterations (NNI) and linear iterations (NLI), for different base grids and different numbers of refinement levels.

	NNI					NLI				
Levels	1	2	3	4	5	1	2	3	4	5
32×32	1.5	2.0	2.0	2.1	2.5	3.4	7.9	12.0	19.3	33.7
64×64	1.8	2.0	2.0	2.4	–	6.5	11.7	19.1	33.2	–
128×128	1.8	2.0	2.4	–	–	12.5	20.1	27.2	–	–
256×256	1.9	2.0	–	–	–	19.9	27.5	–	–	–
512×512	1.9	–	–	–	–	26.3	–	–	–	–

DISCLAIMER

This work was performed under the auspices of the U.S. Department of Energy by Los Alamos National Laboratory, which is operated by the University of California under contract W-7405-ENG-36. Los Alamos National Laboratory does not endorse the viewpoint of a publication or guarantee its technical correctness. LA-UR 05-2645

References

1. S. Balay, W. Gropp, L. C. McInnes, and B. Smith, *PETSc Users Manual*, Tech. Rep. ANL-95/11 - Revision 2.1.6, Argonne National Laboratory, 2004.
2. P. N. Brown and Y. Saad, *Hybrid Krylov methods for nonlinear systems of equations*, SIAM J. Sci. Statist. Comput., 11 (1990), pp. 450–481.
3. L. Chacón and D. A. Knoll, *A 2D high-β hall MHD implicit nonlinear solver*, J. Comput. Phys., 188 (2003), pp. 573–592.
4. L. Chacón, D. A. Knoll, and J. M. Finn, *An implicit, nonlinear reduced resistive MHD solver*, J. Comput. Phys., 178 (2002), pp. 15–36.
5. R. D. Hazeltine, M. Kotschenreuther, and P. J. Morrison, *A four-field model for tokamak plasma dynamics*, Phys. Fluids, 28 (1985), pp. 2466–2477.
6. D. A. Knoll and D. E. Keyes, *Jacobian-free Newton-Krylov methods: a survey of approaches and applications*, J. Comput. Phys., 193 (2004), pp. 357–397.
7. S. McCormick, *Multilevel Adapative Methods for Partial Differential Equations*, SIAM, Philadelphia, PA, 1989.
8. M. Pernice and R. D. Hornung, *Newton-Krylov-FAC methods for problems discretized on locally refined grids*, Comput. Vis. Sci., (2005). (to appear).
9. H. Strauss and D. Longcope, *An adaptive finite element method for magnetohydrodynamics*, J. Comput. Phys., 147 (1998), pp. 318–336.